ChemPubSoc Europe

DOI: 10.1002/ejic.201501343

EurJIC European Journal of Inorganic Chemistry

Full Paper

Charge Transfer Salts

Charge-Transfer Salts Based on a Dissymmetrical Cyano-Substituted Tetrathiafulvalene Donor

Sandrina Oliveira,[a] Isabel C. Santos,[a,b] Elsa B. Lopes,[a] Joana T. Coutinho,[a] Laura C. J. Pereira,[a] Dulce Belo,[a] Sandra Rabaça*[a] and Manuel Almeida*[a]

Abstract: Three salts of the dissymmetrical TTF derivative cyanobenzene-ethylenedithio-tetrathiafulvalene (CNB-EDT-TTF) with different anions, namely, $(CNB\text{-}EDT\text{-}TTF)_2[M(mnt)_2]$ [M = Ni (**1**), Au (**2**); mnt = maleonitriledithiolate] and (CNB-EDT-TTF)$FeBr_4$ (**3**) were prepared and characterized by single-crystal X-ray diffraction, magnetic susceptibility, and electrical conductivity measurements. Compounds **1** and **2** are isostructural with a crystal structure characterized by segregated chains of side-by-side donor dimers and acceptors, and compound **3** presents donors in dimerized stacks. In spite of the different structural types and stoichiometries, all of these compounds have C–N···H pairing interactions associated with $R^2_2(10)$ synthons between donors in nearby chains. All compounds are poor semiconductors, and the magnetic susceptibility of **1** is dominated by the contribution of the paramagnetic $[Ni(mnt)_2]$ anions with small antiferromagnetic interactions. The magnetic susceptibility of **3** is dominated by the paramagnetic $FeBr_4$ anions and follows a Curie–Weiss law with a Weiss temperature θ = –19 K, which denotes significant antiferromagnetic interactions that are most likely mediated by the donors.

Introduction

Recently, it has been shown that the dissymmetrical tetrathiafulvalene (TTF) derivative cyanobenzene-ethylenedithio-tetrathiafulvalene (CNB-EDT-TTF, see Scheme 1)[1] originates a new type of salt with unusual $(CNB\text{-}EDT\text{-}TTF)_4A$ stoichiometry by electrocrystallization in the presence of small anions (A = ClO_4^-, PF_6^-, and I_3^-), and the donors have an unprecedented bilayer structure.[2] This bilayer structure is induced by effective inter-donor interactions through the nitrile groups, associated with a combination of $R^2_2(10)$ and $R^2_2(8)$ synthons with C–N···H interactions, and can provide 2D metallic systems with unusual and interesting properties depending on the layer packing pattern of the donors. However, the factors that control the possible occurrence of these bilayer structures in charge-transfer salts are not entirely clear and remain only very poorly controlled. As the C–N···H interactions involved in the bilayer structure are relatively weak, the formation of the bilayers is expected to be critically dependent on the counteranions. Therefore, it appears of clear interest to explore salts with different anions and see to what extent this bilayer structure and the C–N···H interactions can be preserved in salts with anions of different size, shape, or charge. Therefore, we have selected square-planar bis(dithiolene) anions of $[M(mnt)_2]$ type (mnt = maleonitriledithiolate or *cis*-2,3-dimercapto-2-butenedinitrile, M = Au and Ni) and the large tetrahedral anion $FeBr_4$. With bis(ethylene)dithiotetrathiafulvalene (BEDT-TTF) and related symmetrical donors, these anions lead to structures without layer arrangements of the donors that are entirely different from those observed with small anions and even to different stoichiometries. When combined with BEDT-TTF, the square-planar bis(dithiolene) anions and related donors tend to favor mixed stackings,[3] and the $FeBr_4$ anion leads instead to a 1:1 salt with BEDT-TTF, despite its similarity with smaller tetrahedral anions (e.g., ClO_4 and $FeCl_4$).[4]

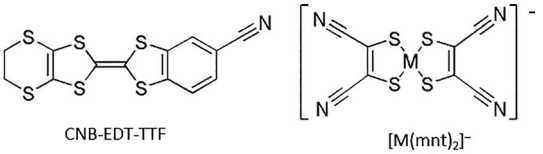

Scheme 1. CNB-EDT-TTF donor and $[M(mnt)_2]^-$ acceptors molecules.

In this paper, we show that the combination of CNB-EDT-TTF with such anions leads to the salts $(CNB\text{-}EDT\text{-}TTF)_2[M(mnt)_2]$ [M = Ni (**1**), Au (**2**)] and (CNB-EDT-TTF)$FeBr_4$ (**3**) with different structural types and stoichiometries, in which the C–N···H donor pairing interactions remain present but in different forms.

Results and Discussion

The charge-transfer salts of CNB-EDT-TTF were prepared by electrocrystallization from dichloromethane solutions, and crys-

[a] *C2TN, Instituto Superior Técnico, Universidade de Lisboa, Estrada Nacional 10, 2695-066 Bobadela LRS, Portugal*
E-mail: sandrar@ctn.tecnico.ulisboa.pt
malmeida@ctn.tecnico.ulisboa.pt
http://www.ctn.tecnico.ulisboa.pt/cvs/qui/uk_cv_srabaca.htm
http://www.ctn.tecnico.ulisboa.pt/cvs/qui/uk_cv_malmeida.htm
[b] *Centro de Química Estrutural, Instituto Superior Técnico, Universidade de Lisboa, 1049-001 Lisboa, Portugal*

Supporting information and ORCID(s) from the author(s) for this article are available on the WWW under http://dx.doi.org/10.1002/ejic.201501343.

Table 1. Crystallographic data for **1**–**3**.[a]

	(CNB-EDT-TTF)$_2$[Ni(mnt)$_2$] (**1**)	(CNB-EDT-TTF)$_2$[Au(mnt)$_2$] (**2**)	(CNB-EDT-TTF)FeBr$_4$ (**3**)
Formula	$C_{34}H_{14}NiN_6S_{16}$	$C_{34}H_{14}AuN_6S_{16}$	$C_{13}H_7Br_4FeNS_6$
Molar mass	1078.18	1214.59	745.05
T [K]	150(2)	150(2)	296(2)
Dimensions [mm]	0.30 × 0.12 × 0.03	0.30 × 0.20 × 0.02	0.20 × 0.1 × 0.02
Crystal system	triclinic	triclinic	triclinic
Space group	$P\bar{1}$	$P\bar{1}$	$P\bar{1}$
a [Å]	6.5758(2)	6.5810(4)	8.1393(18)
b [Å]	10.8313(3)	10.9210(6)	11.411(2)
c [Å]	14.5381(4)	14.5694(8)	11.754(3)
α [°]	107.719(4)	107.142(2)	82.416(7)
β [°]	91.284(2)	91.348(2)	87.398(7)
γ [°]	98.732(2)	98.777(3)	86.035 (8)
Volume [Å^3]	972.32(5)	986.28(10)	1078.8(4)
Z	1	1	2
$\varrho_{calcd.}$ (g/cm^3)	1.841	2.045	2.294
h, k, l range	−7/8, ±13, ±17	−7/8, −12/13, ±17	9/7, −13/103, ±13
θ_{max} [°]	25.68	26.16	25.03
Reflections collected	10411	7803	6796
Reflections indexed	3663	3321	3687
Reflections [$I > 2\sigma(I)$]	3008	3103	1745
R_1	0.036	0.033	0.0675
ωR_2	0.083	0.075	0.201

[a] CCDC 1415877 (for **1**), 1415878 (for **2**), and 1415879 (for **3**) contain the supplementary crystallographic data for this paper. These data can be obtained free of charge from The Cambridge Crystallographic Data Centre.

tals of **1**–**3** were typically obtained under standard galvanostatic conditions after 10 d.

Single crystals of **1**, **2**, and **3** suitable for X-ray diffraction were selected, and their crystallographic data are given in Table 1. The charge-transfer salts **1** and **2** are isostructural and crystallized in the triclinic system, space group $P\bar{1}$, with one independent half anionic unit [M(mnt)$_2$]$^-$ with the metal atom located at an inversion center and one independent cationic CNB-EDT-TTF donor in the unit cell (Figure 1 for **1** and Figure S1 for **2**). A disorder of the CN groups over two positions with occupation factors of 40 % (C17A/N3A) and 60 % (C17/N3) was observed.

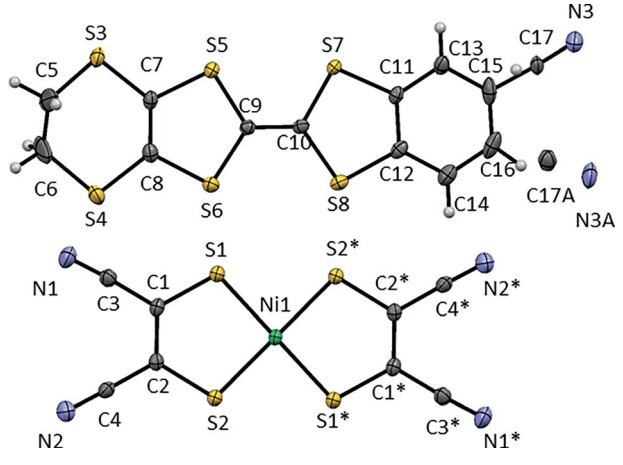

Figure 1. ORTEP diagram of the molecular units in **1** with atomic displacement parameters drawn at the 50 % probability level and the atomic numbering scheme; H atoms have been omitted for clarity [symmetry code: (*) 1 − x, 1 − y, 1 − z].

The donor and acceptor units are essentially planar, and the bond lengths are listed in Tables S1 and S2. The Ni–S (2.144, 2.143 Å) and Au–S bond lengths (2.312, 2.313 Å; see Table S1) are typical of monoanionic [M(mnt)$_2$]$^-$ complexes with M = Ni[5] and Au[6] and identical to those found in related salts.[7] As expected, the donor bond lengths, namely, the central C=C and C–S bonds, which in TTF-type donors are more sensitive to the oxidation state,[8] were intermediate between those of the neutral donor[1] and the fully oxidized donors in salt **3** (see below and Table S2).

The donors are arranged in head-to-tail dimers related by an inversion center at a short interplanar distance (3.540 Å) and with short S8···S5* contacts (* = x, 1 − y, 1 − z) at 3.555 Å that denote strong intradimer π–π interactions (Figure 2, a). These dimers are arranged in chains along a through short side-by-side intermolecular contacts (Figure 2, b). The donor dimers are connected to nearby chains through C–N···H interactions that couple the donors head to head in an almost coplanar position. This interaction can be described as an $R^2_2(10)$ synthon (Figure 3, a), as previously found in the bilayer compounds (CNB-EDT-TTF)$_4$ A and also in other cyano-substituted TTFs[9] and several nitriles. The geometric characteristics of these C–N···H interactions in **1** and **2** are listed in Table 2. The donor (D) dimers

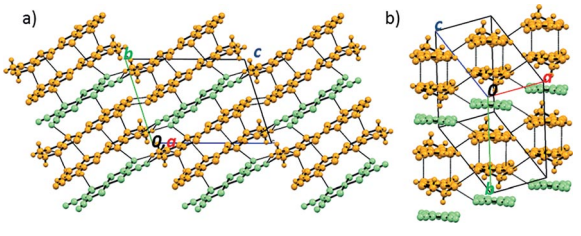

Figure 2. Crystal structure of **1**: (a) view along the a axis; (b) partial view along donor (D) and acceptor (A) molecular long axes of a layer made of parallel molecules stacked ···DDADDA··· along b. The CNB-EDT-TTF molecules are orange, and the [Ni(mnt)$_2$]$^-$ molecules are blue.

alternate with anions (A) to form ···DDADDADDA··· stacks along *b* (Figure 2). The anions also make chains along *a* through side-by-side intermolecular contacts [S2···S2* (* = –*x*, 1 – *y*, 1 – *z*) at 3.631 Å].

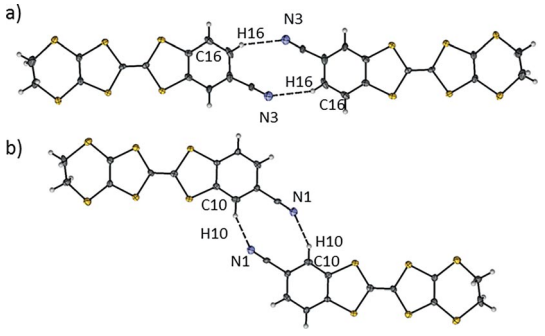

Figure 3. Interdonor contacts associated with $R^2_2(10)$ synthons in (a) **1** and (b) **3**. The bond lengths and angles are listed in Table 2.

Table 2. Short C–H···N contacts in the crystal structures of **1**–**3**.

	Head-to-head contact $R^2_2(10)$	* Symmetry operation	Distance [Å]/angle [°]
1	C16–H16···N3*	2 – *x*, 1 – *y*, 2 – *z*	2.735/138.60
2	C16–H16···N3*	2 – *x*, 1 – *y*, 2 – *z*	2.724/151.20
3	C10–H10···N1*	1 – *x*, 1 – *y*, –*z*	2.623/137.09

Compound **3** crystallizes in the triclinic system in the space group $P\bar{1}$ with one independent $FeBr_4^-$ anion and one independent cationic CNB-EDT-TTF donor in the unit cell (Figure 4). In addition to the usual envelope-type folding of the dithiine group, the donors present a small bending of the central aromatic core. As expected for fully oxidized donors, the central C=C bond the C–S bonds present a larger deviation than those observed for **1** and **2**. As shown in Table S2, as one goes from the neutral donor to the partially oxidized donors (**1** and **2**) and then to fully oxidized donors in **3**, a small but consistent increase in the central C=C bond length is observed together with a decrease of the C–S bond lengths. This is in agreement with molecular orbital calculations, which indicate that the highest occupied molecular orbital (HOMO) of the donor has a bonding character in the central C=C bonds and an antibonding character in the C–S bonds;[2] therefore, the removal of electrons from this HOMO upon donor oxidation leads to the observed bond shortening and lengthening.

The crystal structure of **3** is made of donors stacked head to tail along *a* to form chains of dimers (Figure 5). The donor dimers are formed by S···S, C···C, and C–H···C contacts (see Table 3) with short central interplanar distances of 3.708 Å. The donor stacks are interconnected along *b* by C–N···H interactions similar to those previously observed for this donor, associated again with an $R^2_2(10)$ synthon (see Figure 3, b and Table 2). The $FeBr_4$ anions are located between the donor chains with several short Br···S contacts (see Table 3).

The electrical resistivity (ϱ) of **2** was measured along the needle axis *b* of the crystals with only a two-probe configuration owing to the small sizes of the samples. This limitation is probably not significant in view of the rather low conductivity (9.3×10^{-4} S/cm at room temperature) of this compound, which

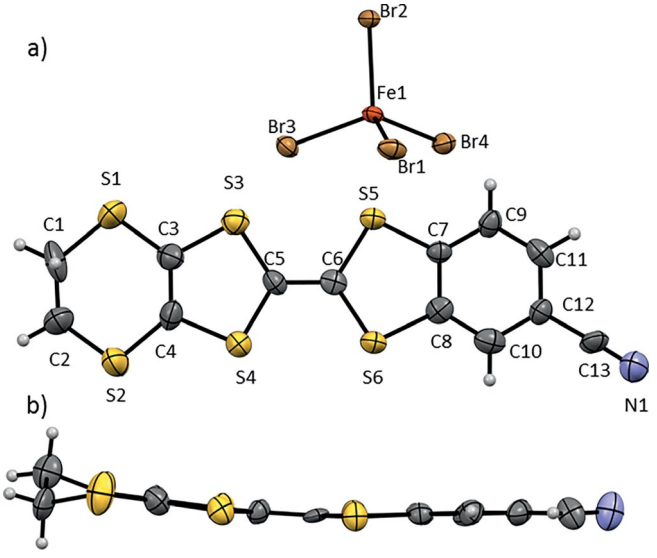

Figure 4. ORTEP diagrams and atomic numbering scheme of charge-transfer salt **3**; atomic displacement parameters are drawn at the 50 % probability level. H atoms have been omitted for clarity.

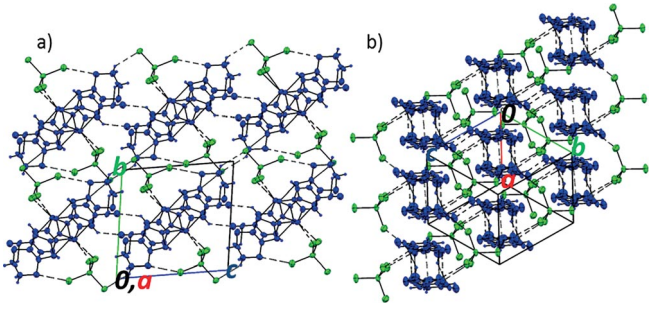

Figure 5. Crystal structure of **3**: (a) view along *a* and (b) partial view along the donor long axis.

Table 3. Short intermolecular contacts between donor (D) and acceptor (A) units in the crystal structure of [CNB-EDT-TTF] $FeBr_4$ (**3**).

	Distance [Å]	Symmetry operation	Type
C13–N1···Br2	3.552	1 – *x*, 1 – *y*, 1 – *z*	D···A
C13–N1···S1	3.537	–1 + *x*, *y*, 1 + *z*	D···D
S3···S6	3.482(5)	–*x*, 1 – *y*, 1 – *z*	D···D
S5···S4	3.493(5)	–*x*, 1 – *y*, 1 – *z*	D···D
C6···C6	3.29(2)	–*x*, 1 – *y*, 1 – *z*	D···D
C1–H1A···C13	2.850	–*x*, 1 – *y*, 1 – *z*	D···D
Br1···S2	3.574(5)	–*x*, 2 – *y*, 1 – *z*	A···D
Br3···S6	3.599(4)	–*x*, 2 – *y*, 1 – *z*	A···D
Br4···S6	3.629(4)	1 – *x*, 2 – *y*, 1 – *z*	A···D
C11–H11···Br2	2.970	1 – *x*, 1 – *y*, 1 – *z*	A···D
C12-H2B···Br2	3.049	–x, 2 – *y*, 2 – *z*	A···D
C10–H10···N1	2.623	1 – *x*, 1 – *y*, –*z*	D···D

follows a semiconducting behavior with a high activation energy (E_a = 257 meV, Figure 6). The thermoelectric power measured along the same direction presents a negative value of ca. –322 μV/K that increases as the temperature decreases (Figure 7) and confirms the semiconducting behavior, as expected from the dimerized arrangement of the donors. A similar semiconducting behavior is expected for the isostructural com-

pound **1**; however, it was not possible to measure the data because of the very small size of the crystals. Compound **3** also presents a semiconducting behavior with an electrical conductivity measured along *a* of 1.5×10^{-3} S/cm at room temperature and an activation energy of 85 meV.

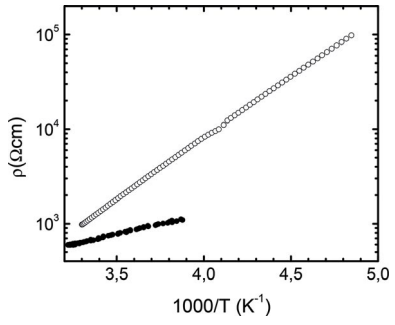

Figure 6. Temperature-dependent electrical resistivity of single crystals of $(CNB\text{-}EDT\text{-}TTF)_2[Au(mnt)_2]$ (open circles) and (CNB-EDT-TTF)$FeBr_4$ (closed circles).

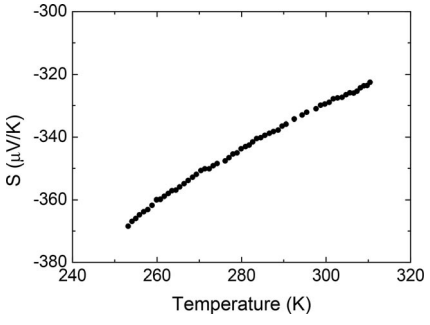

Figure 7. Absolute thermopower, *S*, of single crystals of **2** as a function of temperature.

The poor electrical conductivity and the semiconducting behavior of these compounds can be understood in terms of the intermolecular interactions and the corresponding predictions of the electronic band structure, which can be made initially by the extended Hückel approach.[10] For that purpose, the relevant $\beta_{HOMO-HOMO}$ intermolecular interaction energies,[11] which are a measure of the strength of the interaction between the HOMOs of the different donor molecules in the crystal structure as identified in Figure 8, were calculated with a double-ζ basis set[12] and are reported in Table 4.

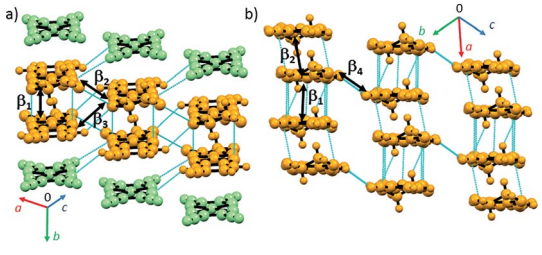

Figure 8. Partial view of the crystal structures of **1** (left) and **3** (right) along the donor long axis. The arrows denote the different relevant interdonor interactions. The CNB-EDT-TTF molecules are orange, and the $[Ni(mnt)_2]^-$ molecules are blue.

The dominant interactions in **1** and **2** are intradimer (β_1) interactions that are one order of magnitude larger than the interdimer interactions (β_2 and β_3) along *a*. Relatively weak β_4 intermolecular interactions between the chains through the C–N···H contacts of the $R^2_2(10)$ synthon are estimated as only 6 and 3 meV in **1** and **2**, respectively. As a consequence of the large intradimer interaction β_1, the donor HOMO of **2** leads to two narrow, essentially one-dimensional, bands (less than 0.1 eV wide) separated by a large gap of 0.33 eV, and the upper band is half-filled (Figure 9). Virtually identical results were obtained for the isostructural compound **1** (Figure S4). Therefore, the poor semiconducting properties observed result from electronic-repulsion energy effects, which are particularly effective in narrow half-filled one-dimensional bands and lead to Mott insulating states.

Table 4. Absolute values of different $\beta_{HOMO-HOMO}$ intermolecular interaction energies [meV] in the crystal structures of $(CNB\text{-}EDT\text{-}TTF)_nX$. (see Figure 8 and text for identification of the interactions).

X	$[Ni(mnt)_2]$	$[Au(mnt)_2]$	$FeBr_4$
β_1	491.9	557.3	626.3
β_2	24.7	27.5	34
β_3	1.3	10.2	–
β_4	6.2	3.7	1.1

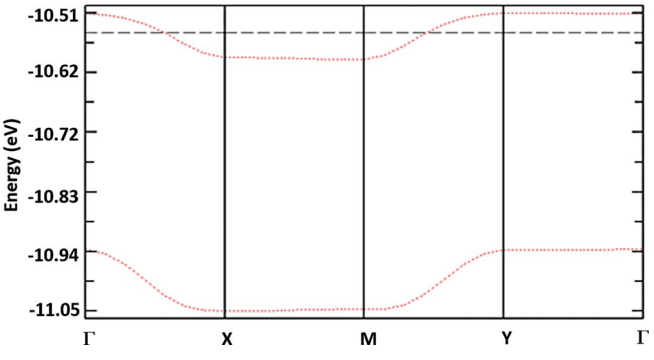

Figure 9. Calculated electronic band structure of **2**. Reciprocal space points $\Gamma = (0, 0, 0)$, $X = (1/2, 0, 0)$, $M = (1/2, 1/2, 0)$, $Y = (0, 1/2, 0)$. The dashed line represents the Fermi level at half of the upper band.

The same type of analysis of the intermolecular interactions in **3** indicates an alternation of strong (β_1 = 626 meV) and weaker (β_2 = 24 meV) interactions along the stacking axis *b* and negligible interstack interactions β_4 through the C–N···H contacts of the $R^2_2(10)$ synthon, estimated as only ca. 1 meV. This strong pairing of the donors in the stacks can be seen as the result of a Peierls distortion in a half-filled band (a chain of fully oxidized radical donors) that leads to an insulating diamagnetic state.

The temperature-dependent paramagnetic susceptibilities of $(CNB\text{-}EDT\text{-}TTF)_2[M(mnt)_2]$ (M = Au, Ni) are shown in Figure 10. The gold salt (**2**) is essentially diamagnetic with a small Curie tail that corresponds to ca. 2 % of $S = 1/2$ impurities. As the $[Au(mnt)_2]^-$ anions are diamagnetic, this result indicates that the donor contribution to the magnetic susceptibility is negligible, probably because of a strong coupling between the donor dimers. In contrast, the nickel salt (**1**) with paramagnetic anions presents a much larger paramagnetic susceptibility with a room-temperature χT of 0.316 emu K/mol, which is slightly lower than the expected value for Ni^{III} ($S = 1/2$, g = 2.00;

0.375 emu K/mol). As the temperature decreases, χT drops gradually until ca. 80 K and then more quickly to reach 0.068 emu K/mol at 4.9 K. The paramagnetic susceptibility can be well-fitted to a Curie–Weiss law, $\chi = C/(T - \theta)$, with C = 0.34 emu K/mol and a negative θ value of –19.4 K. These results indicate that in addition to a negligible donor contribution, as in **2**, the paramagnetic anions in **1** are antiferromagnetically coupled. This antiferromagnetic coupling is not surprising in view of the short side-by-side contacts between the anions, which certainly mediate the magnetic interactions.

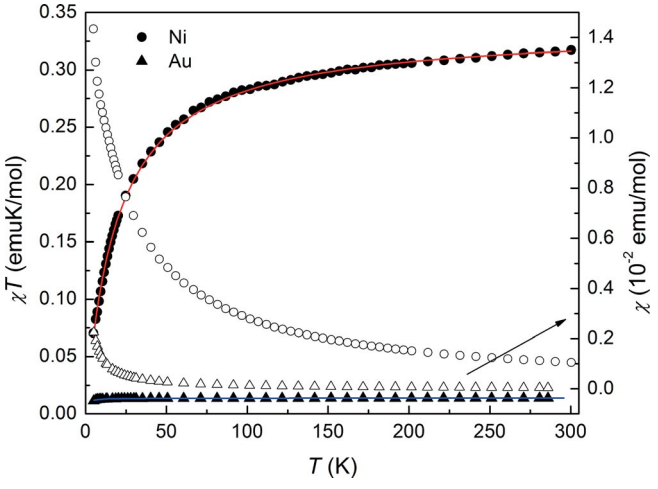

Figure 10. Temperature (T) dependence of the magnetic susceptibility, χ (open symbols) and χT (closed symbols), of (CNB-EDT-TTF)$_2$[M(mnt)$_2$] (triangles: M = Au, circles: M = Ni). The red line is the fit to a Curie–Weiss model with C = 0.34 emu K/mol and θ = –19.4 K for (CNB-EDT-TTF)$_2$[Ni(mnt)$_2$].

The paramagnetic susceptibility of **3** (Figure 11) is dominated by the large contribution of the S = 5/2 $FeBr_4$ anions and can be well-fitted to a Curie–Weiss law for S = 5/2, $\chi = N_A g^2 \mu_B{}^2 S(S + 1)/[3k_B(T - \theta)]$; the experimental g value of 1.96 and the negative θ value of –19.7 K indicate an antiferromagnetic interaction between the spins. This fit corresponds to a C value of 4.14 emu K/mol, which is only slightly lower than that for the ideal system of a high-spin Fe^{III} ion with S = 5/2 and g = 2.0

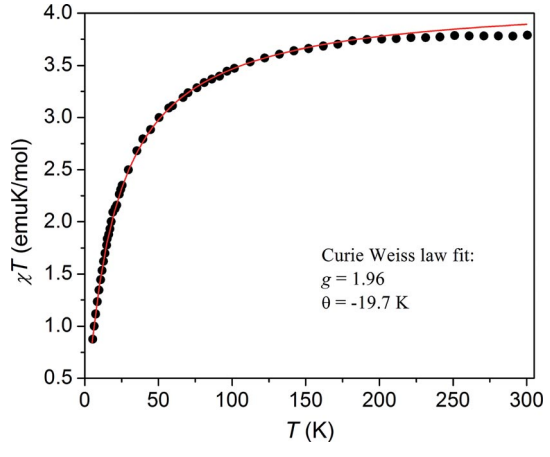

Figure 11. Temperature dependence of the paramagnetic susceptibility product, χT, of (CNB-EDT-TTF)$_2$FeBr$_4$. The red line is the fit to a Curie–Weiss model with C = 4.14 emu K/mol and θ = –19.7 K.

(4.58 emu K/mol), and the experimental g value obtained (1.96) is well within the range found for other $FeBr_4$ compounds.[13]

Notably, the magnitude of this θ value is larger than that observed for the analogous compound with BEDT-TTF (–5 K);[4] therefore, the antiferromagnetic interactions are certainly mediated through the donors. A mechanism of antiferromagnetic interactions between the $FeBr_4$ anions mediated trough the donors has been proposed to explain similar strong interactions in salts with more extended V-shaped donors,[13] although we did not observe any evidence for magnetic ordering at low temperatures in this case.

Conclusions

In a similar way to what happened with BEDT-TTF salts, the combinations of both square-planar [M(mnt)$_2$] anions and the large tetrahedral $FeBr_4$ anions with the electron donor CNB-EDT-TTF lead to salts without layer arrangements of the donors and even to a salt with a different stoichiometry (1:1) for $FeBr_4$. Although the double layer structure observed with smaller anions is no longer present, C–N···H interactions associated with an $R^2_2(10)$ synthon are responsible for the pairing of donor molecules in the structures of these salts. The magnetic properties of the [Ni(mnt)$_2$] and $FeBr_4$ salts are dominated by the contributions of the paramagnetic anions with strong antiferromagnetic interactions, which are most likely mediated through the donors in the $FeBr_4$ compound.

Experimental Section

Synthesis and Electrochemical Crystallization. General Remarks: The synthesis of the electron donor cyanobenzene-ethylenedithio-tetrathiafulvalene (CNB-EDT-TTF) was achieved by a general route for the preparation of nonsymmetrically substituted TTF derivatives by the cross-coupling of two different 1,3-dichalcogenole-2-chalconegones, as we described previously.[1] The (nBu$_4$N)[M(mnt)$_2$] (M = Au and Ni) salts were also synthesized and purified by recrystallization, as described previously,[14] and the tetraethylammonium salt of $FeBr_4$ was prepared by treating $FeBr_3$ with tetraethylammonium bromide in a dry methanol solution. The resulting precipitate was recrystallized from hot methanol to give black rectangular prisms.[4] Electrochemical crystal growth of charge-transfer salts from dichloromethane solutions (2–3 × 10^{-3} M) was performed in conventional H-shaped two-compartment cells separated by Frit glass with Pt electrodes under galvanostatic conditions (0.5–1.5 μA/cm^2). Crystals suitable for single-crystal X-ray diffraction and electron-transport measurements with typical dimensions of up to 2 × 0.4 × 0.01 mm^3 were grown on the anode and collected after 8–15 d. The dichloromethane was purified by standard procedures and freshly distilled just before use.

(CNB-EDT-TTF)$_2$[Ni(mnt)$_2$] (1): A dichloromethane solution of the donor CNB-EDT-TTF and nBu$_4$N [Ni(mnt)$_2$] (both 2 × 10^{-3} M) was added to an H-shaped cell. The system was sealed under nitrogen; after approximately 15 d with a constant current density of 0.5 μA/cm^2 applied, the small dark brown platelet crystals that had grown on the anode were collected.

(CNB-EDT-TTF)$_2$[Au(mnt)$_2$] (2): A dichloromethane solution of the donor CNB-EDT-TTF and nBu$_4$N [Au(mnt)$_2$] (both 2 × 10^{-3} M) was added to an H-shaped cell. The system was sealed under nitrogen;

after approximately 8 d with a constant current density of 0.5 μA/cm^{-2} applied, the dark brown platelet crystals that had grown on the anode were collected.

(CNB-EDT-TTF)FeBr$_4$ (3): A dichloromethane solution of the donor CNB-EDT-TTF and NEt_4FeBr_4 (both 3×10^{-3} M) was added to an H-shaped cell. The system was sealed under nitrogen; after approximately 15 d with the application of an initial current density of 1.5 μA/cm^{-2}, the dark brown platelet crystals that had grown on the anode were collected.

X-ray Diffraction Studies: The data were collected with a Bruker APEX II CCD diffractometer with graphite-monochromated Mo-K_α radiation (λ = 0.71073 Å) in the φ and ω scan modes. A semiempirical absorption correction was performed with SADABS.[15] The data collection, cell refinement, and data reduction were performed with the SMART and SAINT programs.[16] The structures were solved by direct methods with SIR97[17] and refined by full-matrix least-squares methods with the program SHELXL97[18] and the winGX software package.[19] Non-hydrogen atoms were refined with anisotropic thermal parameters, whereas H atoms were placed in idealized positions and allowed to ride on their parent C atom. Molecular graphics were prepared with ORTEP 3.[20]

Electrical Transport Measurements: The thermoelectric power and resistivity measurements of single crystals were performed in the temperature range 200–310 K by using a measurement cell attached to the cold stage of a closed-cycle helium refrigerator. The thermopower was measured by a slow alternating current (AC, ca. 10–2 Hz) technique[21] by attaching two 25 μm diameter 99.99 % pure Au wires (Goodfellow metals) thermally anchored to two quartz reservoirs with Pt paint (Demetron 308A) to the extremities of an elongated sample, as in a previously described apparatus,[22] and the system was controlled by a computer.[23] The oscillating thermal gradient was kept below 1 K and measured with a differential Au (0.05 atom-% Fe) versus chromel thermocouple of the same type. The absolute thermoelectric power of the sample was obtained after correction for the absolute thermopower of the Au leads by using the data of Huebner.[24] The electrical conductivities were measured with the same setup by using a two-contact configuration with a Keithley 619 electrometer.

Electronic Structure Calculations: The electron band structures and intermolecular interaction energies were calculated by employing the extended Hückel method.[10a,25]The basis set consisted of Slater-type orbitals of double-ξ quality. A modified Wolfsberg–Helmholz formula was used to calculate the nondiagonal H_{ij} terms.[10]

Magnetic Measurements: The magnetic susceptibilities of polycrystalline samples of (CNB-EDT-TTF)[M(mnt)$_2$] (M = Ni, Au; ca. 10 mg) were measured with an S700X superconducting quantum interference device (SQUID) magnetometer (Cryogenic Ltd.) in the temperature range 2–300 K under a magnetic field of 1 T. These measurements were corrected for the diamagnetic contributions of each compound, which were estimated from tabulated Pascal constants as -511×10^{-6}, -539×10^{-6}, and -227.1×10^{-6} emu/mol for **1**–**3**, respectively.

Acknowledgments

This work was supported by the Portuguese Fundação do Ministério de Ciência e Tecnologia (FCT) through contracts PTDC/QUI QUI/101788/2008 and PTDC/QEQ-SUP/1413/2012. The C2TN/IST authors gratefully acknowledge the FCT support through the UID/Multi/04349/2013 project. S. O. is thankful to FCT for the PhD grant SFRH/BD/86131/2012.

Keywords: Sulfur heterocycles · Noncovalent interactions · Charge transfer · Electrical properties · Magnetic properties

[1] S. Oliveira, D. Belo, I. C. Santos, S. Rabaça, M. Almeida, *Beilstein J. Org. Chem.* **2015**, *11*, 951–956.
[2] S. Oliveira, J. Ministro, I. C. Santos, D. Belo, E. B. Lopes, S. Rabaça, E. Canadell, M. Almeida, *Inorg. Chem.* **2015**, *54*, 6677–6679.
[3] a) W. Reith, K. Polborn, E. Amberger, *Angew. Chem. Int. Ed. Engl.* **1988**, *27*, 699–670; *Angew. Chem.* **1988**, *100*, 722; b) J. Tarés, M. Mas, E. Molins, J. Veciana, C. Rovira, J. Morgado, R. T. Henriques, M. Almeida, *J. Mater. Chem.* **1995**, *5*, 1653–1658; c) M. Fettouhi, A. Waheed, S. Golhen, N. Helou, L. Ouahab, P. Molinié, *Synth. Met.* **1999**, *102*, 1764–1765; d) T. Devic, B. Domercq, P. Auban-Senzier, P. Molinié, M. Fourmigué, *Eur. J. Inorg. Chem.* **2002**, 2844–2849; e) M. Mas-Torrent, H. Alves, E. B. Lopes, M. Almeida, K. Wurst, J. Vidal-Gancedo, J. Veciana, C. Rovira, *J. Solid State Chem.* **2002**, *168*, 563–572; f) X. Chi, B. Scott, G. Lawes, A. P. Ramirez, *J. Chem. Crystallogr.* **2004**, *34*, 249–253.
[4] T. Mallah, C. Hollis, S. Bott, M. Kurmoo, P. Day, M. Allan, R. H. Friend, *J. Chem. Soc., Dalton Trans.* **1990**, 859–865.
[5] G. R. Lewis, I. Dance, *J. Chem. Soc., Dalton Trans.* **2000**, 3176–3185.
[6] J. C. Fitzmaurice, A. M. Z. Slawin, D. J. Williams, J. D. Woollins, *Polyhedron* **1990**, *9*, 1561–1565.
[7] R. A. L. Silva, A. I. S. Neves, E. B. Lopes, I. C. Santos, J. T. Coutinho, L. C. J. Pereira, C. Rovira, M. Almeida, D. Belo, *Inorg. Chem.* **2013**, *52*, 5300–5306.
[8] a) P. Guionneau, C. J. Kepert, G. Bravic, D. Chasseau, M. R. Truter, M. Kurmoo, P. Day, *Synth. Met.* **1997**, *86*, 1973–1974; b) T. Mori, A. Kobayashi, Y. Sasaki, H. Kobayashi, G. Saito, H. Inokuchi, *Bull. Chem. Soc. Jpn.* **1984**, *57*, 627.
[9] T. Devic, J. N. Bertran, B. Domercq, E. Canadell, N. Avarvari, P. Auban-Senzier, M. Fourmigué, *New J. Chem.* **2001**, *25*, 1418–1424.
[10] a) M.-H. Whangbo, R. Hoffmann, *J. Am. Chem. Soc.* **1978**, *100*, 6093–6098; b) J. H. Ammeter, H.-B. Burgi, J. Thibeault, R. Hoffmann, *J. Am. Chem. Soc.* **1978**, *100*, 3686–3692; c) J. Ren, W. Liang, M.-H. Whangbo, *Crystal and Electronic Structure Analysis Using CAESAR*, PrimeColor Software, Inc., Cary, NC, **1998**.
[11] M.-H. Whangbo, J. M. Williams, P. C. W. Leung, M. A. Beno, T. J. Emge, H. H. Wang, *Inorg. Chem.* **1985**, *24*, 3500–3502.
[12] a) E. Canadell, I. E.-I. Rachidi, S. Ravy, J. P. Pouget, L. Brossard, J. P. Legros, *J. Phys.* **1989**, *50*, 2967–2981;: b) S. Baudron, N. Avarvari, E. Canadell, P. Auban-Senzier, P. Batail, *Chem. Eur. J.* **2004**, *10*, 4498–4511.
[13] T. Kominami, T. Matsumoto, K. Ueda, T. Sugimoto, K. Murata, M. Shiroc, H. Fujita, *J. Mater. Chem.* **2001**, *11*, 2089–2094.
[14] a) A. Davison, N. Edelstein, R. H. Holm, A. H. Maki, *Inorg. Chem.* **1963**, *2*, 1227–1232; b) A. Davison, R. H. Holm, *Inorg. Synth.* **1967**, *10*, 8–26.
[15] G. M. Sheldrick, *SADABS*, Bruker AXS Inc., Madison, WI, **2004**.
[16] *SMART* and *SAINT*, Bruker AXS Inc., Madison, WI, **2004**.
[17] A. Altomare, M. C. Burla, M. Camalli, G. Cascarano, G. Giacovazzo, A. Guagliardi, A. G. G. Moliterni, G. Polidori, R. Spagna, *J. Appl. Crystallogr.* **1999**, *32*, 115–119.
[18] G. M. Sheldrick, *SHELXL97*, *Program for Crystal Structure Refinement*, University of Göttingen, Germany, **1997**.
[19] L. J. Farrugia, *J. Appl. Crystallogr.* **1999**, *32*, 837–838.
[20] L. J. Farrugia, *J. Appl. Crystallogr.* **1997**, *30*, 565.
[21] P. M. Chaikin, J. F. Kwak, *Rev. Sci. Instrum.* **1975**, *46*, 218–220.
[22] M. Almeida, S. Oostra, L. Alcácer, *Phys. Rev. B* **1984**, *30*, 2839–2844.
[23] E. B. Lopes, *INETI-Sacavém*, internal report, **1991**.
[24] R. P. Huebner, *Phys. Rev. A* **1964**, *135*, A1281–A1921.
[25] R. J. Hoffmann, *Chem. Phys.* **1963**, *39*, 1397–1412.

Received: November 18, 2015
Published Online: February 16, 2016